

Cascaded silicon micro-ring modulators for WDM optical interconnection

Qianfan Xu, Brad Schmidt, Jagat Shakya, and Michal Lipson

*School of Electrical and Computer Engineering
Cornell University, Ithaca, NY 14853
lipson@ece.cornell.edu*

Abstract: We experimentally demonstrate cascaded silicon micro-ring modulators as the key components of a WDM interconnection system. We show clean eye-diagrams when each of the four micro-ring modulators is modulated at 4 Gbit/s. We show that optical inter-channel crosstalk is negligible with a channel spacing of 1.3 nm.

©2006 Optical Society of America

OCIS codes: (130.3120) Integrated optics devices; (230.2090) Electro-optical devices; (250.5300) Photonic integrated circuits

References and Links

1. D. A. B. Miller, Optical interconnects to silicon. *IEEE J. Sel. Top. Quantum Electron.* **6**, 1312–1317 (2000).
2. J. D. Meindl, J. A. Davis, P. Zarkesh-Ha, C. S. Patel, K. P. Martin, and P. A. Kohl, “Interconnect opportunities for gigascale integration,” *IBM Res. Dev.* **46**, 245–263 (2002).
3. K. K. Lee, D. R. Lim, and L. C. Kimerling, “Fabrication of ultralow-loss Si/SiO₂ waveguides by roughness reduction,” *Opt. Lett.* **26**, 1888–1890 (2001).
4. Y. A. Vlasov, and S. J. McNab, “Losses in single-mode silicon-on-insulator strip waveguides and bends,” *Opt. Express* **12**, 1622–1631 (2004). <http://www.opticsexpress.org/abstract.cfm?URI=OPEX-12-8-1622>.
5. A. Liu, R. Jones, L. Liao, D. Samara-Rubio, D. Rubin, O. Cohen, R. Nicolaescu, and M. Paniccia, “A high-speed silicon optical modulator based on a metal-oxide-semiconductor capacitor,” *Nature* **427**, 615–618 (2004).
6. G. Gunn, “CMOS photonicsTM - SOI learns a new trick,” in *Proceedings of IEEE International SOI Conference* (Institute of Electrical and Electronics Engineers, New York, 2005), pp. 7–13.
7. Q. Xu, B. Schmidt, S. Pradhan, and M. Lipson, “Micrometre-scale silicon electro-optic modulator,” *Nature* **435**, 325–327 (2005).
8. O.I. Dosunmu, D.D. Cannon, M.K. Emsley, L.C. Kimerling, and M.S. Unlu, “High-speed resonant cavity enhanced Ge photodetectors on reflecting Si substrates for 1550-nm operation,” *IEEE Photon. Technol. Lett.* **17**, 175–177 (2005).
9. T. Sadagopan, S. J. Choi, S. J. Choi, K. Djordjev, and P. D. Dapkus, “Carrier-induced refractive index changes in InP-based circular microresonators for low-voltage high-speed modulation,” *IEEE Photon. Technol. Lett.* **17**, 414–416 (2005).
10. T. Sadagopan, S. J. Choi, S. J. Choi, P. D. Dapkus, and A. E. Bond, “Optical Modulators Based on Depletion Width” *IEEE Photon. Technol. Lett.* **17**, 567–569 (2005).
11. P. Rabeii, W. H. Steier, C. Zhang, and L. R. Dalton, “Polymer Micro-Ring Filters and Modulators,” *J. Lightwave Technol.* **20**, 1968–1975 (2002).
12. N. Pleros, C. Bintjas, M. Kalyvas, G. Theophilopoulos, K. Yiannopoulos, S. Sygletos, and H. Avramopoulos, “Multiwavelength and power equalized SOA laser sources,” *IEEE Photon. Technol. Lett.* **14**, 693–695 (2002).
13. Teik-Kooi Ong, Ming Yin, Zheng Yu, Yuen-Chuen Chan, and Yee-Loy Lam “High performance quantum well intermixed superluminescent diodes,” *Meas. Sci. Technol.* **15**, 1591–1595 (2004).
14. R. A. Soref, and B. R. Bennett, “Electrooptical effects in silicon,” *IEEE J. Quantum Electron.* **23**, 123–129 (1987).
15. M. S. Rasras, D. M. Gill, S. S. Patel, A. E. White, K. Tu, Y. Chen, D. N. Carothers, A. T. Pomerene, M. J. Grove, D. Sparacin, J. Michel, M. A. Beals, and L. C. Kimerling, “Tunable Narrowband Optical Filter in CMOS,” in *Proceedings of Optical Fiber Communication Conference and the National Fiber Optic Engineers Conference* (Institute of Electrical and Electronics Engineers, New York, 2006), PDP13.
16. B. E. Little, J. T. Laine, and S. T. Chu, “Surface-roughness-induced contradirectional coupling in ring and disk resonators,” *Opt. Lett.* **22**, 4–6 (1997).
17. T. J. Kippenberg, S. M. Spillane, and K. J. Vahala, “Modal coupling in traveling-wave resonators,” *Opt. Lett.* **27**, 1669–1671 (2002).

18. M. Borselli, T. J. Johnson, and O. Painter, "Beyond the Rayleigh scattering limit in high-Q silicon microdisks: theory and experiment," *Opt. Express* **13**, 1515-1530 (2005).
19. Qianfan Xu, Vilson Almeida, and Michal Lipson, "Micrometer-scale all-optical wavelength converter on silicon", *Opt. Lett.* **30**, 2733-2735 (2005).
20. M. Notomi and S. Mitsugi, "Wavelength conversion via dynamic refractive index tuning of a cavity," *Phys. Rev. A* **73**, 051803 (2006).
21. S. F. Preble, Q. Xu, B. S. Schmidt, and M. Lipson, "Ultrafast all-optical modulation on a silicon chip," *Opt. Lett.* **30**, 2891-2893 (2005).

Optical interconnections on silicon have been extensively investigated in recent years as interconnections become the bottleneck for the next-generation computing systems [1,2]. The goal of these investigations is to provide a compact, low-power-consumption, high bandwidth and low-latency optical interconnection system with full CMOS-compatibility. Silicon based optical components such as low-loss silicon-on-insulator (SOI) optical waveguides [3,4], high-speed silicon modulators [5-7], and Ge-on-SOI detectors [8] have been demonstrated, enabling large-scale optical integration on a silicon chip. While most attention is focused on single-channel systems at this stage, wavelength division multiplexing (WDM) technology is necessary to fully utilize the ultra-wide bandwidth of the optical interconnection medium, given that the transmission bandwidths of both silicon waveguides and optical fibers are on the order of 10-100 THz. In this paper, we present a simple architecture for a WDM interconnection system based on silicon ring resonators. As the key components of such a system, we show high-speed and multi-channel modulation using cascaded silicon micro-ring modulators.

The silicon modulator is a key component for CMOS-compatible optical interconnection systems. Recently, high-speed modulators based on free-carrier plasma dispersion effect have been demonstrated using either Mach-Zehnder interferometers (MZI) [5,6] or micro-ring resonators [7,9,10] in silicon and III-V materials. Comparing to the mm-long MZI-based modulators, the advantages of the ring-resonator-based modulator include its small size (~ 10 μm) and low-power consumption. In the ring resonator, in contrast to single-pass devices like MZI, light at the resonant wavelength travels many round trips in the resonator, and interacts with the carriers many times. As a result, the total number of carriers needed to change the optical transmission of the ring resonator is much less than that needed in MZI-modulators, and therefore much less RF power is needed to drive these carriers in and out of the active region.

For the WDM interconnection systems, in addition to the low power consumption and small size, ring modulators have another advantage: they modulate only light at particular wavelengths (the resonant wavelengths of the ring resonators) and allow light at all other wavelengths to pass through the modulators without been affected. Therefore, one can cascade several ring modulators with different resonant wavelengths on a single waveguide, and modulate different wavelengths of light independently. Fig. 1 shows a simple architecture for a WDM interconnection system. A similar structure has been proposed for polymer modulators [11]. Light from a WDM source [12] or a broadband source [13] is sent into a silicon waveguide coupled to multiple ring modulators with different resonant wavelengths. If the input is a WDM source, the resonant wavelength of each modulator needs to match the wavelength of each channel of the WDM source. At the receiver side, these channels can be demultiplexed using similar ring resonators with drop ports, and detected separately. If the input is a broadband source, it only requires that the resonant wavelengths of the ring modulators match one-to-one with those of the ring demultiplexers.

The key components of the WDM interconnection system are the cascaded modulators shown in the shadowed area of Fig. 1, which are fabricated on a SOI substrate. The device structure is based on the micro-ring modulator we presented in ref. 7. They consist of ring resonators embedded with PIN junctions used to inject and extract free carriers, which in turn modify the refractive index of the silicon and the resonant wavelength of the ring resonator using the mechanism of the plasma dispersion effect [14]. The waveguides and rings are

formed by silicon strips with the height of 200 nm and the width of 450 nm on top of a 50-nm-thick slab layer. In ref. 7, the speed of the modulator was limited to 400 Mbps under non-return-to-zero (NRZ) coding. The reason for this limitation is that the p-i-n junction is formed on only part of the ring resonator, while carriers diffuse into the section of the ring that is not part of the p-i-n junction, where they can not be efficiently extracted during the reverse biased period, leading to a longer fall time following consecutive '1's. In the new design presented here, an additional n⁺-doped region is added outside of the straight waveguide to form nearly closed p-i-n junctions. This new geometry ensures that all carriers injected into the ring can be extracted efficiently by reversely biasing the junction. The distance between the doped regions and the edge of the ring resonators and straight waveguides is reduced from ~1 μm in ref. 7 to ~300 nm to further increase the extraction speed with the same reverse bias voltage. The fabrication process is similar to that described in ref. 7. The radii of the four ring resonators are designed to be 4.98 μm, 5.00 μm, 5.02 μm, and 5.04 μm, respectively. The difference in the radii corresponds to a channel spacing of 3.6 nm. A top-view microscopic picture of two of the four fabricated ring modulators is shown in Fig. 2. The image shows both the ring resonators coupled to the straight waveguide and the metal pads contacting the doped regions.

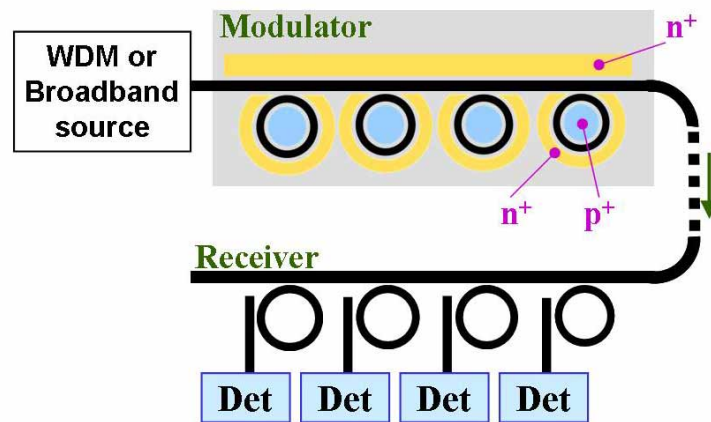


Fig. 1. Schematics of a WDM optical interconnection system with cascaded silicon ring resonators as a WDM modulator and demultiplexer. Det: detector.

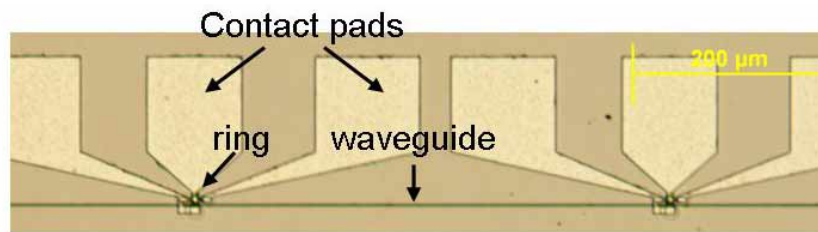


Fig. 2. Top-view microscopic picture of the fabricated modulators, showing two of the four ring modulators coupled to a straight waveguide.

Figure 3 shows the TE-mode transmission spectrum of the waveguide coupled to the four ring modulators measured with a tunable laser. At the resonant wavelength of each ring resonator, light is coupled into the ring resonator and lost due to scattering from the side-wall roughness of the resonator, causing a spectral dip at the resonant wavelength. The resonances of the four rings can be identified on the spectrum, which are marked by numbers 1 to 4 on the spectrum. The quality factors (Q) of the resonators are around 20,000. By changing the refractive index of the ring, thereby tuning the resonance wavelength, [7] four data channels can be modulated at the four resonant wavelengths by the ring modulators. One can see that the resonant wavelengths of the four modulators are not equally spaced. The variation of the

resonant wavelength of each ring resonator is mainly due to fabrication imperfections. This fabrication-induced variation of resonant wavelength can be compensated with local heating of each ring resonator using integrated heaters [15]. Ring 3 and 4 have smaller extinction ratios as the results of under-coupling, and slight double-dip features because of the coupling between clockwise and counter-clockwise traveling modes, which is caused by roughness-induced back-reflection in the ring resonator [16-18]. The dip-splitting is ~ 0.03 nm for ring 3 and ~ 0.05 nm for ring 4.

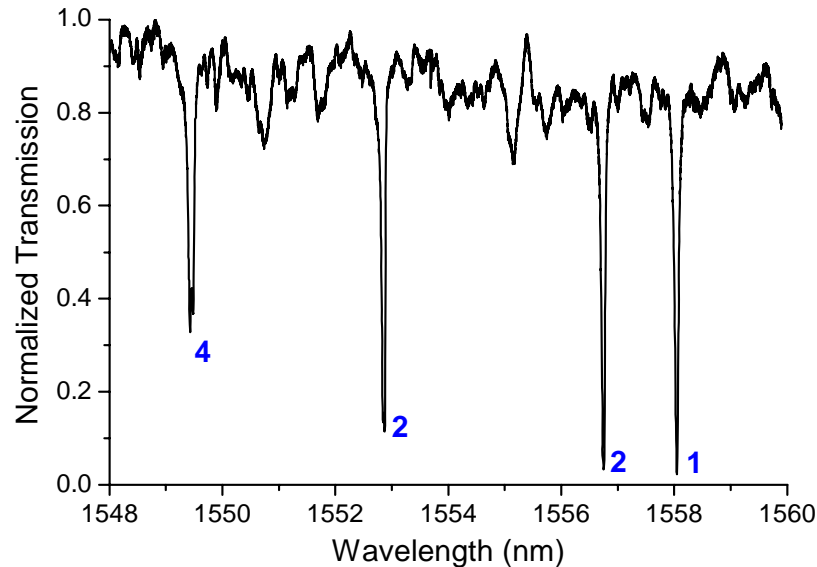


Fig. 3. Normalized transmission spectrum of the waveguide coupled to the 4 micro-ring modulators. The resonances of the four rings are identified and marked on the spectrum.

Figure 4 shows the eye-diagrams of the modulated outputs of the four channels, measured with a 12-GHz detector. Each ring modulator is tested separately. Pseudo-random NRZ data (PRBS $2^{10}-1$) from a pattern generator is amplified by a wide-band RF amplifier and applied on each device using an RF probe. The output peak-to-peak voltage of the RF amplifier is ~ 6.5 V, and the DC bias is set at -1.0 V. The data rate of each channel is 4 Gbit/s. The extinction ratios for channel 1 and 2 are ~ 13 dB. The extinction ratios for channel 3 and 4 are less than 10 dB as expected from the transmission spectrum. From the eye-diagram, one can see that the rise and fall times of the modulator are around 40 ps and 60 ps respectively, suggesting a possible modulation speed beyond 10 Gbit/s. When the data rate is increased above 5 Gbit/s, however, we observed a large jittering at the rising edge. We found that this is due to the distortion of the electrical signal originating from the impedance mismatch between the off-chip driving system and the device. This problem can be solved by using an integrated RF driver for the modulator. In the experiment, a wideband microwave amplifier with 6.5 V peak-to-peak output voltage is used to drive the modulator. The relatively high driving voltage is needed mainly due to the high contact resistance of the fabricated device (~ 10 k Ω). The contact resistance can be greatly reduced by optimizing the doping profile and annealing condition for the contacts.

On the eye-diagrams, one can see an overshoot on every rising edge of the signal. While a small portion of this overshoot is due to the response of the optical detector, most of the overshoot comes from the inherent property of the ring modulator when the rising time is comparable to the photon lifetime of the resonator. When the resonator is at the on-resonance state with low optical transmission, light is trapped inside the resonator with high optical intensity [19]. The optical transmission at this state is low because the light coupled back from the ring resonator destructively interfere with the directly transmitted light in the output waveguide. When the cavity is tuned from the on-resonance state to off-resonance state, the

input light is transmitted through the device with little coupling to the ring resonator. At the same time, light trapped inside the resonator is slightly wavelength shifted due to the temporal change of refractive index. This wavelength shifted was recently shown theoretically in [20]. Because of the wavelength shift, instead of destructively interfering with the uncoupled input wave, the trapped light couples back into the output waveguide and beats with the input wave, resulting in an overshoot and damped oscillation. The frequency of the damped oscillation is proportional to the wavelength shift of the trapped light and the damping rate is determined by the photon lifetime of the resonator (~ 17 ps in the tested device).

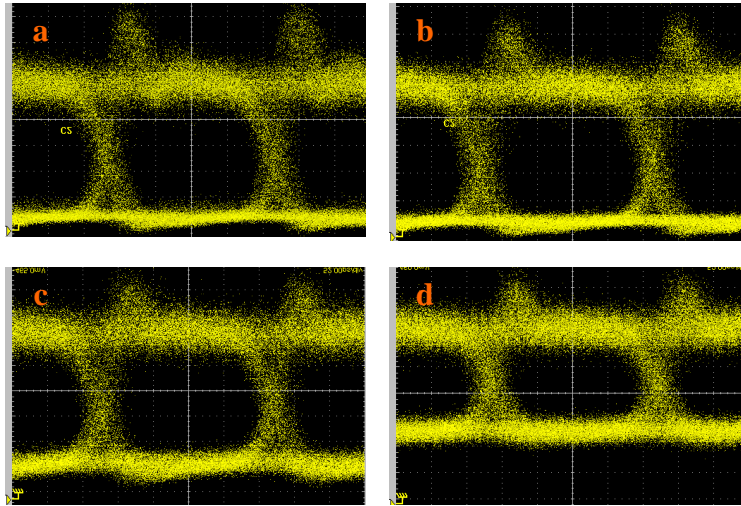


Fig. 4. Eye-diagrams of the modulated optical output of the four channels at 4 Gbit/s. (a): channel 1 at 1558.1 nm. (b): channel 2 at 1556.8 nm. (c): channel 3 at 1552.9 nm. (d): channel 4 at 1549.5 nm.

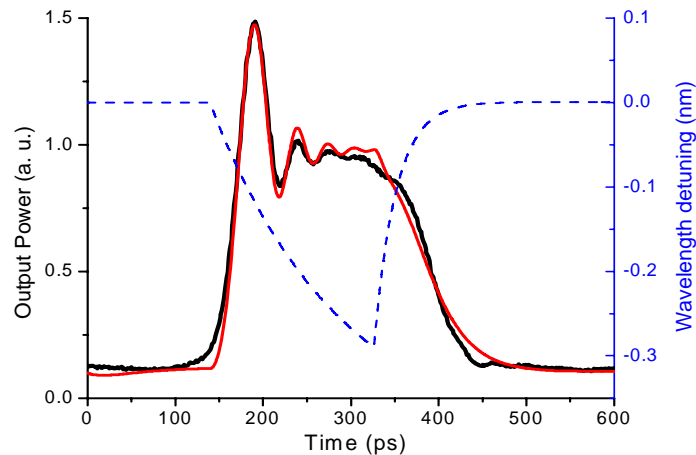


Fig. 5. Waveform of a bit '1' in a pseudo-random bit sequence at the bit-rate of 6 Gbit/s. Black line: measured output optical power. Red line: simulated output optical power. Blue dotted line (associated with the right y-axis): the temporal change of resonant wavelength of the ring resonator assumed in the simulation.

This beating between the trapped light and the transmitted light at the rising edge of the modulated optical output can be seen more clearly on the averaged waveforms taken with a 30-GHz detector. The black line in Fig. 5 shows the waveform of a bit '1' at 6 Gbit/s in the modulated optical output. The overshoot and the damped oscillation as the result of the beating are evident. We simulated the transmission of the ring resonator using a time-domain

model by assuming the temporal shift of the resonant wavelength of the ring resonator follows the blue dotted line in Fig. 5, which consists of two exponential decay curves with time constants determined by the speed of carrier injection and extraction. As fitting parameters we use time constants of 150 ps and 30 ps for the carrier injection and extraction, respectively. The extraction time is consistent with the experimental value measured in [21]. The overshoot and damped oscillation features are reproduced very well in the simulated waveform, as the red line in Fig. 5 shows. From the eye-diagrams in Fig. 4, one can see that the overshoot and the residue oscillation have little effect on the openness of the eyes. From the red line in fig. 5, one can also see the high transmission stabilized at around 0.98, slightly less than 1, corresponding to a 0.1-dB insertion loss from the residue coupling to the ring resonator.

In order to test the possible crosstalk between different channels, we analyze channels 1 and 2 with the closest channel spacing of 1.3 nm. When ring 1 is modulated at 4 Gbit/s with output waveform shown as the black line in Fig. 6, the wavelength of the input laser is tuned close to the resonance of ring 2. The blue, green and red line shows the optical output when the laser is on the resonant wavelength, at the edge of the resonance, and just outside the resonance of ring 2, respectively. No significant modulation is observed on any of the three waveforms, showing the absence of optical crosstalk between channels 1.3 nm apart. This indicates that there are no fundamental limitations for fitting at least 14 channels into the 18-nm free-spectral range (FSR) of the modulator. Theoretical analysis shows that the channel spacing can be reduced to below 0.6 nm without optical inter-channel crosstalk. Note that the FSR of the ring resonator can be increased by reducing the size of the ring resonator. A ring with a diameter of 3 μm would support more than 50 channels.

In conclusion, we demonstrate cascaded silicon ring modulators as the key components of a simple architecture for a WDM interconnection system. From the measured performance of the modulators, higher than 50×10 Gbit/s data bandwidth can be expected in such a system.

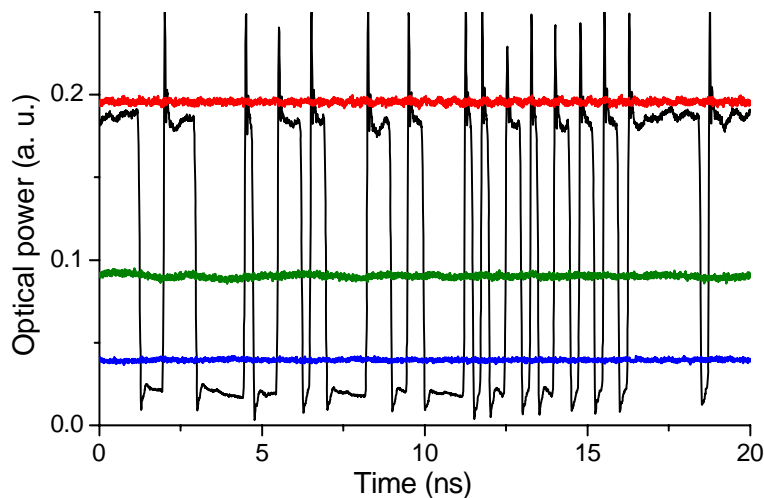


Fig. 6. Waveforms when ring 1 is modulated at 4 Gbit/s. Black line: output waveform at the resonant wavelength of ring 1. Blue line: output waveform at the resonant wavelength of ring 2. Green line: output waveform at the edge of ring-2 resonance. Red line: output waveform just outside of ring-2 resonance.

Acknowledgments

This work has been partially carried out as part of the Interconnect Focus Center Research Program at Cornell University, supported in part by the Microelectronics Advanced Research Corporation (MARCO), its participating companies. The modulator geometry development was sponsored by the Defense Advanced Research Projects Agency's EPIC program supervised by Drs. Jagdeep Shah and Richard Soref. The program is executed by the Microsystems Technology Office (MTO) under Contract No. HR0011-05-C-0027.